GEOPHYSICAL RESEARCH LETTERS, VOL. 40, 380–385, doi:10.1029/2012GL054620, 2013

Trends and variations of ocean surface latent heat flux: Results from GSSTF2c data set

Si Gao,[1] Long S. Chiu,[1] and Chung-Lin Shie[2,3]

Received 7 November 2012; revised 27 November 2012; accepted 29 November 2012; published 31 January 2013.

[1] Trends and variations of Goddard Satellite-based Surface Turbulent Fluxes (GSSTF) version 2c (GSSTF2c) latent heat flux (LHF) are examined. This version of LHF takes account of the correction in Earth incidence angle. The trend of global mean LHF for GSSTF2c is much reduced relative to GSSTF version 2b Set 1 and Set 2 for the same period 1988–2008. Temporal increase of GSSTF2c LHF in the two decades is 11.0%, in which 3.1%, 5.8%, and 2.1% are attributed to the increase in wind, the increase in sea surface saturated air humidity, and the decrease in near-surface air humidity, respectively. The first empirical orthogonal function of LHF is a conventional El Niño Southern Oscillation (ENSO) mode. However, the trends in LHF are independent of conventional ENSO phenomena. After removing ENSO signal, the pattern of LHF trends is primarily determined by the pattern of air-sea humidity difference trends.
Citation: Gao, S., L. S. Chiu, and C.-L. Shie (2013), Trends and variations of ocean surface latent heat flux: Results from GSSTF2c data set, *Geophysical Res. Lett.*, *40*, 380–385, doi:10.1029/2012GL054620.

1. Introduction

[2] Ocean surface latent heat flux (LHF), or evaporation multiplied by the latent heat of evaporation, is a crucial component in global water and energy cycles. It also plays an important role in salinity budget of the upper ocean. Accurate observations of ocean surface LHF are essential in understanding ocean-atmosphere interactions on different scales, forcing ocean and coupled models, and studying the ocean heat and fresh water budget.

[3] In a bulk aerodynamic algorithm, LHF is determined by the transfer coefficient of evaporation, C_E, and bulk parameters such as surface wind speed (U), surface saturated and near-surface air specific humidity (Q_s and Q_a),

$$LHF = \rho L_v C_E U(Q_s - Q_a) \quad (1)$$

where Q_s is determined by sea surface temperature (SST) and salinity, ρ is density of moist air, and L_v is latent heat of vaporization. The transfer coefficient is dependent on the stability of the atmosphere and the sea state [*Liu et al*., 1979; *Zeng et al*., 1998].

[4] To study trend and variability of oceanic evaporation, reliable long-term global data sets are desirable. The International Comprehensive Ocean-Atmosphere Data Set offers the most complete surface marine observations since 1662, mainly from ships and buoys [*Woodruff et al*., 2011]. However, the International Comprehensive Ocean-Atmosphere Data Set based LHF parameters have serious spatial and temporal sampling problems (measurements over the ship lanes can introduce a fair weather bias) as well as measurement uncertainty [e.g., *Chou et al*., 2003]. Reanalysis from numerical weather prediction models provide another source of LHF. These reanalysis data are produced by the forecast cycles that are highly dependent on physical parameterizations, and are not strongly nor widely constrained by observations.

2. Data

[5] Satellite observations provide global monitoring of the bulk variables. For instance, data collected by the Special Sensor Microwave Imager (SSM/I) on board the Defense Meteorological Satellite Program satellites have been used to retrieve near-surface air humidity and winds over the ocean, and have been the basis of various satellite-based LHF products. These products include the Goddard Satellite-based Surface Turbulent Fluxes (GSSTF) data set [*Chou et al*., 1997; *Chou et al*., 2003], the Japanese Ocean Flux data sets with Use of Remote Sensing Observations (J-OFURO) [*Kubota et al*., 2002] and the Hamburg Ocean Atmosphere Parameters and Fluxes from Satellite Data (HOAPS) [*Grassl et al*., 2000]. LHF estimates from Objectively Analyzed air-sea Fluxes (OAFlux) data set [*Yu and Weller*, 2007] are also made available by merging satellite and reanalysis data.

[6] Large trends in these LHF products have been noted in the satellite products. *Chiu et al*. [2008] argued that the dominant nonseasonal variation may be related to a decadal variation of the Hadley circulation and El Niño-Southern Oscillation (ENSO), respectively. *Liu and Curry* [2006] suggested that LHF trend in OAFlux during 1989–2000 was associated primarily with an increasing surface wind speed. *Yu* [2007] found a transition from a downward trend to an upward trend in LHF around 1977–1978 and emphasized the dominant role of the wind forcing in this decadal change. *Yu and Weller* [2007] argued that the positive surface LHF trend for the period 1981–2005 is primarily linked to an increasing SST. *Li et al*. [2011] argued that the positive LHF trend during 1977–2006 in the tropical and subtropical Pacific

[1]Department of Atmospheric, Oceanic and Earth Sciences, George Mason University, Fairfax, Virginia, USA.
[2]Joint Center for Earth Systems Technology, University of Maryland, Baltimore County, Baltimore, Maryland, USA.
[3]NASA Goddard Space Flight Center, Greenbelt, Maryland, USA.

Corresponding author: L. S. Chiu, Department of Atmospheric, Oceanic and Earth Sciences, George Mason University, Fairfax, VA, USA. (lchiu@gmu.edu)

0094-8276/13/2012GL054620

was closely associated with both the SST warming and the surface wind speed strengthening.

[7] The role of surface air humidity, Q_a, in determining the trends in the earlier versions of GSSTF was noted [*Shie*, 2010, 2011; *Chiu et al*., 2012]. Reanalyzed Q_a is used as an input for producing OAFlux and that is a major uncertainty due to the lack of direct observations [*Yu and Weller*, 2007]. An updated version of SSM/I version 6 (V6) data released by Remote Sensing Systems in 2006 (as used by *Wentz et al*. [2007], see http://www.ssmi.com) that calibrates all SSM/I sensors is available in 2008. *Shie et al*. [2010] reprocessed and forward processed GSSTF2 to version GSSTF2b using the SSM/I V6 data (including total precipitable water, brightness temperature, and wind speed retrieval), covering the period July 1987 to December 2008. Two sets of GSSTF2b are available, Set 1, which is compiled from all data from the SSM/I series, and Set 2, which excludes SSM/I data sets that are deemed to show large trends. New versions of other products based on SSM/I V6 data have also been released, such as HOAPS version 3 (HOAPS3) and J-OFURO version 2 (J-OFURO2). A comparison of these updated data sets in terms of trends and variability has been examined by *Chiu et al*. [2012].

[8] Analyses of GSSTF2b products [*Shie*, 2010] revealed relatively large (positive) trends in LHF, particularly post year 2000, which was mainly due to the (negative) trends found in the SSM/I V6 brightness temperature (*Tb*). *Hilburn and Shie* [2011] showed that drifts and variations in satellite attitude have not been properly accounted for in the SSM/I V6 *Tb*, resulting in geolocation and Earth incidence angle (EIA) errors. EIA correction applied to *Tb* resulted in a considerably reduced decreasing trend of the boundary layer water vapor [*Hilburn and Shie*, 2011]. The latest version of GSSTF2, GSSTF2c [*Shie et al*., 2011; *Shie*, 2011], incorporates the corrected *Tb* resulting from applying a simple and accurate correction method developed by *Hilburn and Shie* [2011]. However, unlike the (original) SSM/I V6 *Tb*, the wind speed and total precipitable water had already been EIA corrected [*Wentz*, 1997; *Wentz and Meissner*, 2000] prior to productions of GSSTF2b and GSSTF2c. The goal of this study is to document the improvement of the GSSTF2c product and provide an estimate of the various components that contribute to trends in LHF data sets.

3. Results

3.1. Trends and Spatial Variations

[9] Figure 1 shows the time series of latitude-weighted quasi-globally (60°N–60°S) averaged LHF of GSSTF2c during 1988–2008. Time series for GSSTF2b Set 1 and Set 2 are also included from *Chiu et al*. [2012]. The linear trends in GSSTF2b Set 1 and Set 2 LHF are 10.45 and 7.08 W m^{-2} decade^{-1}, respectively, and the trend in GSSTF2c LHF is reduced to 5.15 W m^{-2} decade^{-1}. The linear LHF trends presented here are qualitatively and quantitatively consistent to the globally (90°N–90°S) averaged LHF trends addressed in *Shie* [2011]. Empirical mode decomposition has also been performed and the results confirm the trends in all three time series.

[10] The linear trends of nonseasonal GSSTF2c LHF for the entire period 1988–2008 are depicted in Figure 2. The monthly climatology data (i.e., January to December) attained from the entire period are removed from the

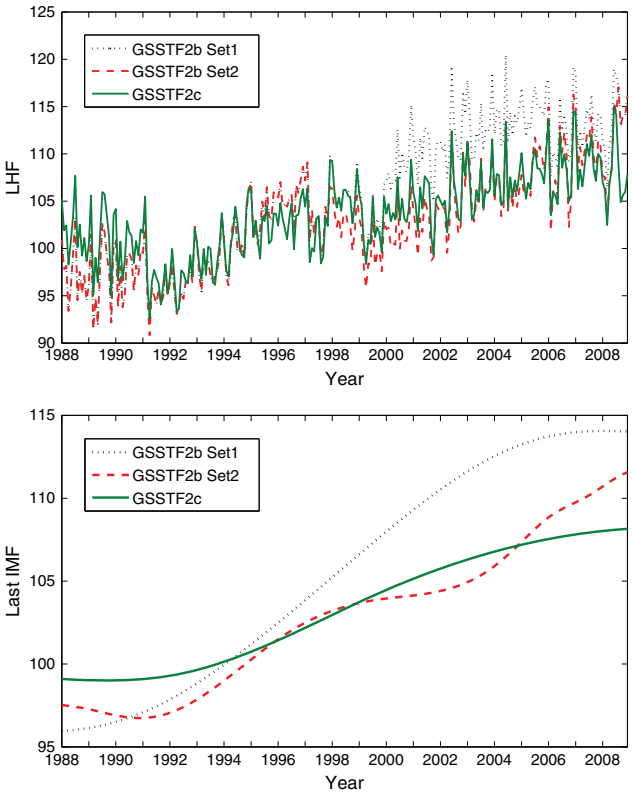

Figure 1. (top) Time series and (bottom) last intrinsic mode functions of quasi-globally (60°N–60°S) averaged oceanic latent heat flux (LHF) derived from GSSTF2b Set 1 and Set 2 and GSSTF2c. Unit in W m^{-2}.

associated individual monthly data to obtain the nonseasonal data set. The maximum increasing trends occur in the storm tracks in the North Atlantic and North Pacific (e.g., in the western boundary current regions of the Gulf Stream and Kuroshio, respectively), the oceanic dry zones off the Inter-tropical Convergence Zone (ITCZ) in South Pacific Ocean, and in latitude bands between 15°S and 40°S in the Indian Ocean, off the coasts of southern and western Australia (particularly in the South Pacific Ocean) and South America (particularly in South Atlantic Ocean).

3.2. Contributing Factors

[11] Variations in C_E are small [*Black et al*., 2007; *DeCosmo et al*., 1996; *Fairall et al*., 2003]. With this assumption, LHF is a product of U and the humidity difference ($DQ = Q_s - Q_a$). Judging from the change pattern of U and DQ they are essentially decoupled. Equation (1) can be integrated globally to get

$$\frac{\delta\overline{LHF}}{\overline{LHF}} \approx \frac{\delta\overline{U}}{\overline{U}} + \frac{\delta\overline{DQ}}{\overline{DQ}} \tag{2}$$

$$\delta\overline{DQ} = \delta\overline{Q_s} - \delta\overline{Q_a} \tag{3}$$

where $\delta\bar{x}$ represents the change in the quantity $\bar{x}$, $\delta\bar{x}/\bar{x}$ represents fractional changes in $\bar{x}$, and the over-bar $\bar{x}$ represents global average of x. For GSSTF2 (1988–2000), the terms in equation (2) are approximately 17%, 6%, and

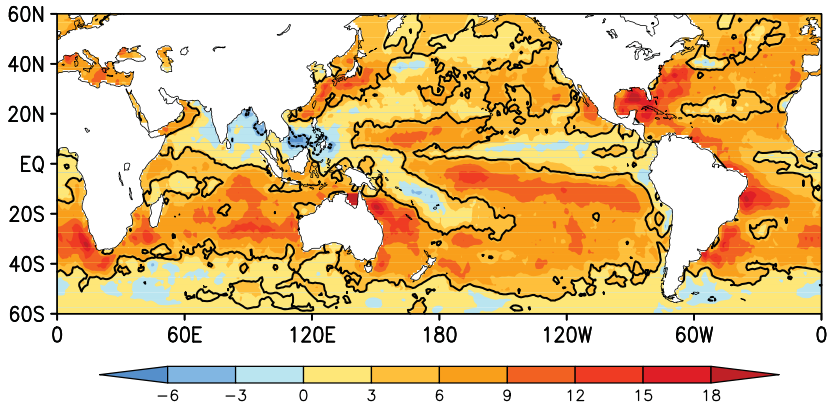

Figure 2. Linear trends of GSSTF2c LHF (1988–2008). Unit in $W\,m^{-2}$ $decade^{-1}$. Contours give the trends above 95% confidence level.

Table 1. Summary of Changes in Quasi-globally (60°N–60°S) Averaged LHF, U and DQ and Q_s and Q_a for HOAPS3 and J-OFURO2 During the Period 1988–2005, and OAFlux, GSSTF2b Set 1 and Set 2, and GSSTF2c During the Period 1988–2008

	$\frac{\delta LHF}{LHF}$	$\frac{\delta \bar{U}}{\bar{U}}$	$\frac{\delta D\bar{Q}}{D\bar{Q}}$	$\delta D\bar{Q}$ ($g\,kg^{-1}$)	$\delta \bar{Q}_s$ ($g\,kg^{-1}$)	$\delta \bar{Q}_a$ ($g\,kg^{-1}$)
HOAPS3	13.7%	5.0%	8.2%	0.30	0.38	0.08
J-OFURO2	15.0%	0.6%	14.3%	0.50	0.26	–0.24
OAFlux	3.3%	3.5%	0.1%	0.004	0.226	0.222
GSSTF2b Set1	23.1%	3.1%	20.0%	0.73	0.22	–0.51
GSSTF2b Set2	15.5%	3.1%	12.3%	0.46	0.22	–0.24
GSSTF2c	11.0%	3.1%	7.9%	0.30	0.22	–0.08

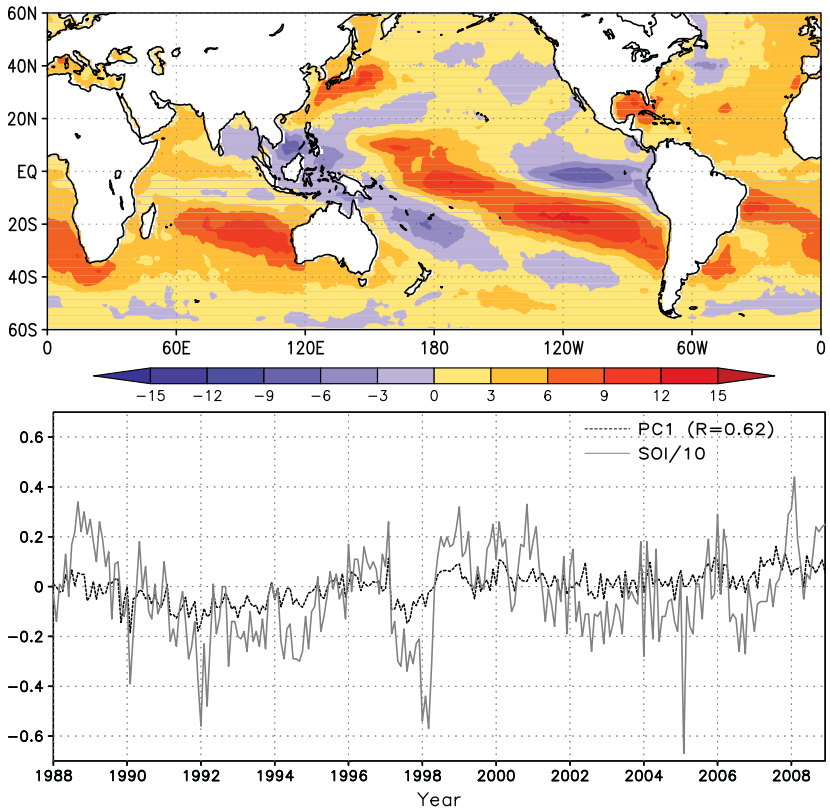

Figure 3. The first EOF pattern (EOF1, top) and its associated time series (PC1, bottom) of nonseasonal GSSTF2c LHF for the period 1988–2008. The variance explained by EOF1 is 5.6%. The South Oscillation Index (SOI) divided by 10 is also shown with PC1. Correlation between PC1 and SOI is 0.62.

11%, in that order [*Xing*, 2006]. Most of the increase in $\overline{DQ}$ was attributed to increase in $\overline{Q_s}$ and decrease in $\overline{Q_a}$.

[12] Table 1 summarizes the changes in global (60°N–60°S) average LHF and the associated changes in U, DQ and the changes in Q_s and Q_a for GSSTF2c during 1988–2008. Results for Set 1 and Set 2 of GSSTF2b, HOAPS3, J-OFURO2, and OAFlux from *Chiu et al.* [2012] are also shown for comparison. These changes were computed without the assumption of C_E invariant. We computed monthly OAFlux Q_s from daily SST data of OAFlux using the Coupled Ocean-Atmosphere Response Experiment 3.0 bulk algorithm. The change in DQ contributes most to the change in LHF, while the change in DQ is due both to increase in Q_s and decrease in Q_a except for HOAPS3. The difference is that changes in Q_s and Q_a have different contributions to changes in DQ for different data sets. The change of DQ for GSSTF2b Set 1 is most attributed to Q_a, and Q_s and Q_a show almost the same contribution to the change of DQ for GSSTF2b Set 2 and J-OFURO2, while Q_s attributes most to the change in DQ for GSSTF2c. It clearly indicates that the LHF trend is reduced because the artificial trend of Q_a has properly been removed in GSSTF2c.

[13] We can further obtain the absolute ratio of the contributions to $\delta\overline{DQ}$ by $\delta\overline{Q_a}$ and $\delta\overline{Q_s}$ in GSSTF2c, i.e., $\delta\overline{Q_a}/\delta\overline{Q_s} = -0.08/0.22 \sim -0.364$. Hence, we can write

$$\delta\overline{DQ}/\overline{DQ} = \left(\delta\overline{Q_s} - \delta\overline{Q_a}\right)/\overline{DQ} \tag{4}$$

and solve for the respective contributions of $\delta\overline{Q_s}$ and $\delta\overline{Q_a}$ to the total change of global average LHF. Among the overall 11.0% changes in LHF, 3.1% is found attributed to wind speed increase, 5.8% to sea surface air humidity (due to SST increase), and 2.1% to near-surface air humidity (decrease).

3.3. Empirical Orthogonal Function Analysis

[14] An empirical orthogonal function (EOF) analysis is performed on nonseasonal LHF of GSSTF2c for the period 1988–2008. The first EOF mode (EOF1) is the only distinct mode based on the method of *North et al.* [1982] and EOF1 is significant by an empirical test of *Craddock and Flood* [1969], and it explains 5.6% of the total variance. Figure 3 indicates the spatial pattern of the EOF1 and the first principal component time series (PC1) accompanied by a rescaled Southern Oscillation Index (SOI). EOF1 is characterized by large positive anomalies over the central equatorial Pacific and southeastern subtropical Pacific associated with large negative anomalies over the maritime continents, western tropical Pacific, and South Pacific Convergence Zone. This pattern is very similar to the second EOFs of GSSTF2 [*Chiu et al.*, 2008] and GSSTF2b Set 1 and Set 2 [*Chiu et al.*, 2012]. The time series of EOF1 is significantly correlated (0.62) with SOI, indicating that EOF1 is an ENSO mode.

[15] It is noteworthy that the first EOF modes of LHF for GSSTF2b Set 1 and Set 2 over the same period [see *Chiu et al.*, 2012], which shows opposite anomalies between the South China Sea and other oceans and the associated time series indicate increasing decadal trends, is no longer the dominant mode in GSSTF2c LHF.

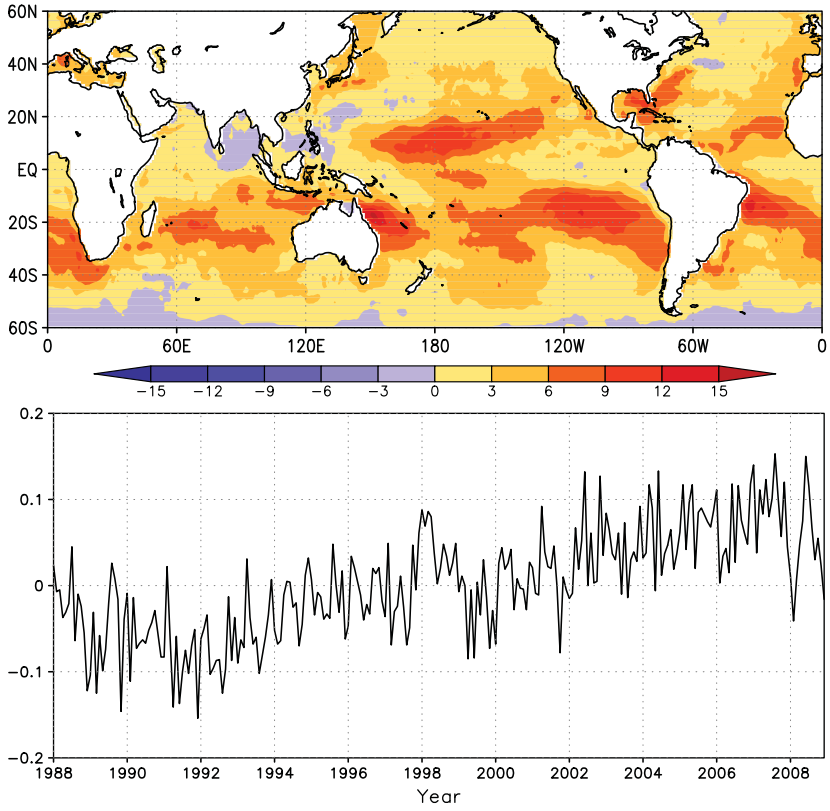

Figure 4. The first EOF pattern (EOF1, top) and its associated time series (PC1, bottom) of nonseasonal GSSTF2c LHF for the period 1988–2008 after ENSO signal is removed. The variance explained is 4.9%.

[16] Does the decadal mode still exist but simply weakens in strength relative to the ENSO mode? To ascertain this decadal mode, the ENSO signal (SOI) is first removed on each grid of nonseasonal LHF by forming a new variable *LHF**,

$$LHF* = LHF - SOI \times \mathrm{cov}(LHF, SOI)/\mathrm{var}(SOI) \quad (5)$$

where cov and var represent the temporal covariance between two variables and the variance, respectively [*An*, 2003]. An EOF analysis is then performed on the new variable *LHF**. This technique effectively removes the ENSO signal in the LHF data set. Figure 4 shows the first EOF (denoted EOF1*) and its associated time series (PC1*) of *LHF**. It is the only distinct and significant mode. The pattern of EOF1* is similar to the trend pattern in Figure 2. PC1* indicates a significant increasing trend and is strongly correlated with LHF time series in Figure 1 (the correlation coefficient is 0.88). This result indicates that trend in GSSTF2c LHF is independent of ENSO, consistent with the finding of *Liu and Curry* [2006] for a shorter period.

[17] To examine the contribution of variables (*U* or *DQ*) to the LHF trend without ENSO impact, EOF analysis is also performed on nonseasonal *U* and *DQ* fields after removing ENSO signal, as was done in equation (5). The first EOF (EOF1) of *DQ*, which is the only distinct and significant mode, is indicated in Figure 5 along with its time series (PC1). This EOF1 pattern is similar to both the EOF1 of LHF in Figure 4 and the LHF trend map in Figure 2, while PC1 of *DQ* shows a significant increasing trend possessing significant correlations of 0.88 and 0.84 with PC1 of LHF (in Figure 4) and LHF time series (in Figure 1), respectively. However, there is no distinct EOF mode found in nonseasonal *U*, because PC1 of *U* does not show a significant trend. These results suggest that the pattern of LHF trend is attributable to *DQ* when discarding ENSO impact.

4. Summary and Discussion

[18] A new version of GSSTF, GSSTF2c, which takes account of the correction in EIA in the SSM/I data, is analyzed to examine the trend and variability of LHF. The trend of global mean LHF for GSSTF2c is 5.15 W m^{-2} decade^{-1}, which is much reduced relative to GSSTF2b Set 1 (10.45 W m^{-2} decade^{-1}) or GSSTF2b Set 2 (7.08 W m^{-2} decade^{-1}) for the same period 1988–2008.

[19] Temporal change of GSSTF2c LHF in the two decades is 11.0%, in which 3.1% is attributed to the change in wind and 7.9% is attributed to the change in air-sea humidity difference (*DQ*). The change in *DQ* is due both to increase in Q_s and decrease in Q_a, and contribution of Q_s is nearly three times as much as that of Q_a, i.e., 5.8% vs. 2.1%. The trend in Q_a is much reduced compared to its predecessor versions. Based on this result, we concluded that the trends in GSSTF2c (11.0%) are mostly attributed to wind and Q_s. The contribution due to changes in Q_a is small (2.1%, or 19% of total change) compared to the other components. The EIA correction in the SSM/I sensors reduce the trend in Q_a. The trends in boundary layer water vapor (W_B) used in the Q_a retrieval decrease from –0.227 mm/decade (used in GSSTF2b, Set 2) to –0.0679 mm/decade (used in GSSTF2c) due to the EIA correction [*Shie and Hilburn*, 2011; *Hilburn and Shie*, 2011].

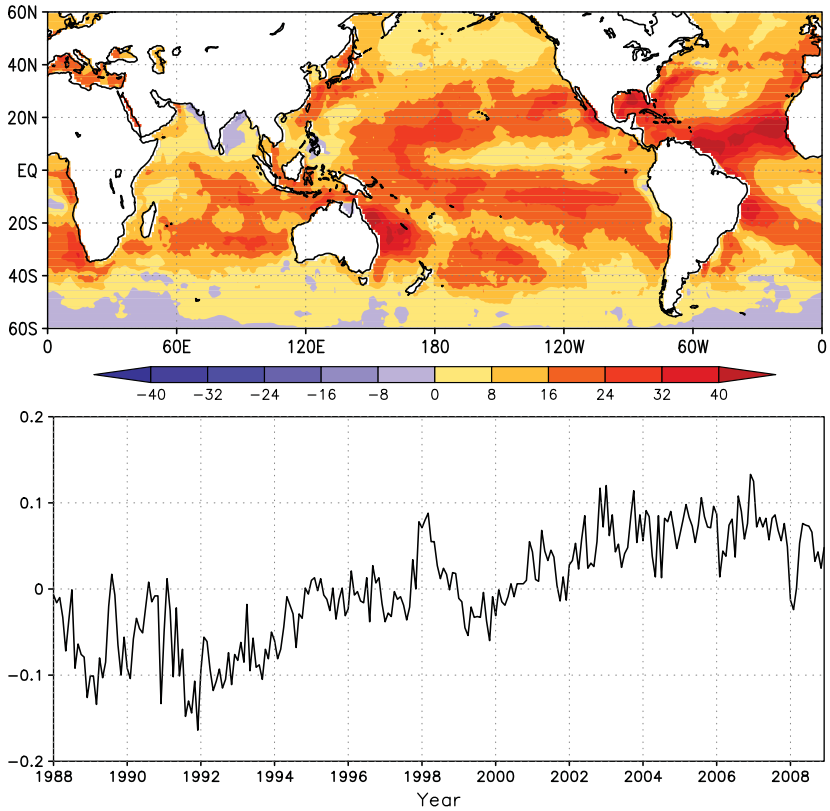

Figure 5. Same as Figure 4 except for air-sea humidity difference ($Q_s - Q_a$). The variance explained is 5.4%.

[20] The first EOF of LHF is a conventional ENSO mode. However, the trends in LHF are independent of conventional ENSO phenomena. After removing ENSO signal, the pattern of LHF trends is primarily determined by the pattern of *DQ* trends.

[21] Among the six data sets, *U* trend of J-OFURO2 is the lowest. *U* of J-OFURO2 is obtained from a combination of microwave radiometers (SSM/I, AMSR-E, and TMI) and scatterometers (ERS-1, ERS-2, and QuikSCAT) while *U* in GSSTF2c and HOAPS3 are mostly based on SSM/I. Comparison of surface wind speed over the Kuroshio region with in situ observations show relatively lower biases for SSM/I F13 and AMSR-E winds compared to J-OFURO2 [*Tomita et al*., 2010].

[22] The change in Q_s is rather consistent among data sets while there are large differences in Q_a change. Q_s is forced by the SST and surface salinity. Q_a change in OAFlux (0.22 g/kg) suggests mostly a thermodynamic response to the increase of SST; both show increases of the right direction and order of magnitude. GSSTF2c and HOAP3 show relatively little change (–0.08 and 0.08 g/kg, respectively) while J-OFURO2 shows the largest negative change (–0.24 g/kg), which may suggest an atmospheric-dynamic origin of the response. The Q_a changes also highlight the major difference between the mostly satellite-based analyses and merged analysis.

[23] **Acknowledgments**. We benefitted from discussions with Drs. M. Kubota and L. Yu. This work was supported by the NASA MEaSUREs program. We thank program manager M. Maiden and program scientist J. Entin for their support of this research. The comments of two anonymous reviewers are also appreciated.

References

An, S.-I. (2003), Conditional maximum covariance analysis and its application to the tropical Indian Ocean SST and surface wind stress anomalies, *J. Climate*, *16*, 2932–2938, doi:10.1175/1520-0442(2003)016<2932:CMCAAI>2.0.CO;2.

Black, P. G., E. A. D'Asaro, W. M. Drennan, J. R. French, T. B. Sanford, E. J. Terrill, P. P. Niiler, E. J. Walsh, and J. Zhang (2007), Air-sea exchange in hurricanes: Synthesis of observations from the Coupled Boundary Layer Air-Sea Transfer experiment, *Bull. Amer. Meteor. Soc.*, *88*, 357–374, doi:10.1175/BAMS-88-3-357.

Chiu, L., R. Chokngamwong, Y. Xing, R. Yang, and C.-L. Shie (2008), "Trends" and variations of global oceanic evaporation data sets from remote sensing, *Acta Oceanol. Sin.*, *27*, 124–135.

Chiu, L., S. Gao, and C.-L. Shie (2012), Oceanic evaporation: trends and variabilities, in *Remote Sensing - Applications*, edited by B. Escalante-Ramirez, pp. 261-278, InTech, Rijeka, Croatia.

Chou, S. H., C.-L. Shie, R. M. Atlas, and J. Ardizzone (1997), Air-sea fluxes retrieved from special sensor microwave imager data, *J. Geophys. Res.*, *102*, 12705–12726, doi:10.1029/97JC00978.

Chou, S. H., E. Nelkin, J. Ardizzone, R. M. Atlas, and C. L. Shie, (2003), Surface turbulent heat and momentum fluxes over global oceans based on the Goddard Satellite retrievals, version 2 (GSSTF-2), *J. Climate*, *16*, 3256–3273, doi:10.1175/1520-0442(2003)016<3256:STHAMF>2.0.CO;2.

Craddock, J. M., and C. R. Flood (1969), Eigenvectors for representing the 500 mb geopotential surface over the Northern Hemisphere, *Quart. J. R. Meteor. Soc.*, *95*, 576–593, doi:10.1002/qj.49709540510.

DeCosmo, J., K. B. Katsaros, S. D. Smith, R. J. Anderson, W. A. Oost, K. Bumke, and H. Chadwick (1996), Air-sea exchange of water vapor and sensible heat: The Humidity Exchange Over the Sea (HEXOS) results, *J. Geophys. Res.*, *101*(C5), 12,001–12,016, doi:10.1029/95JC03796.

Fairall, C. W., E. F. Bradley, J. E. Hare, A. A. Grachev, and J. B. Edson (2003), Bulk parameterization of air–sea fluxes: Updates and verification for the COARE algorithm, *J. Climate*, *16*, 571–591, doi: 10.1175/1520-0442(2003).016<0571:BPOASF>2.0.CO;2.

Grassl, H., V. Jost, M. R. Ramesh Kumar, J. Schulz, B. Bauer, and P. Schluessel (2000), The Hamburg Ocean Atmosphere Parameters and Fluxes from Satellite data (HOAPS): a climatological Atlas of satellite derived air–sea interaction parameters over the oceans. Max Planck Report. No. *312*, 130 pp.

Hilburn, K. A., and C.-L. Shie (2011), Decadal trends and variability in Special Sensor Microwave Imager (SSM/I) brightness temperatures and Earth incidence angle. Report No. 092811, Remote Sensing Systems, 53 pp.

Li, G., B. Ren, C. Yang, and J. Zheng (2011), Revisiting the trend of the tropical and subtropical Pacific surface latent heat flux during 1977–2006, *J. Geophys. Res.*, *116*, D10115, doi:10.1029/2010JD015444.

Liu, J., and J. A. Curry (2006), Variability of the tropical and subtropical ocean surface latent heat flux during 1989–2000, *Geophys. Res. Lett.*, *33*, L05706, doi:10.1029/2005GL024809.

Liu, W. T., K. B. Katsaros, and J. A. Businger (1979), Bulk parameterizations of air-sea exchanges of heat and water vapor including molecular constraints at the interface, *J. Atmos. Sci.*, *36*, 1722–1735, doi: 10.1175/1520-0469(1979)036<1722:BPOASE>2.0.CO;2.

Kubota, M., N. Iwasaka, S. Kizu, M. Konda, and K. Kutsuwada (2002), Japanese ocean flux datasets with use of remote sensing observations (J-OFURO), *J. Oceanogr.*, *58*, 213–225, doi:10.1023/A:1015845321836.

North, G. R., T. L. Bell, R. F. Cahalan, and F. J. Moeng (1982), Sampling errors in the estimation of empirical orthogonal functions. *Mon. Wea. Rev.*, *110*, 699–706, doi:10.1175/1520-0493(1982)110<0699:SEITEO>2.0.CO;2.

Shie, C.-L., L. S. Chiu, R. Adler, I.-I. Lin, E. Nelkin, and J. Ardizzone (2010), The Goddard Satellite-Based Surface Turbulent Fluxes Dataset --- Version 2b (GSSTF2b), In: NASA Goddard Earth Sciences (GES) Data and Information Services Center (DISC), October 2010. Available from ftp://aurapar1u.ecs.nasa.gov/data/s4pa/GSSTF/ or <http://disc.sci.gsfc.nasa.gov/daac-bin/DataHoldingsMEASURES.pl?PROGRAM_List=ChungLinShie>

Shie, C.-L. (2010), Science background for the reprocessing and Goddard Satellite-based Surface Turbulent Fluxes (GSSTF2b) Data Set for Global Water and Energy Cycle Research, In: NASA GES DISC, 18 pp, October 12, 2010. Available from < http://disc.sci.gsfc.nasa.gov/measures/documentation/Science-of-the-data.pdf>

Shie, C.-L. (2011), Science background for the reprocessing and Goddard Satellite-based Surface Turbulent Fluxes (GSSTF2c) Data Set for Global Water and Energy Cycle Research, In: NASA GES DISC, 19 pp, October 28, 2011. Available from <http://disc.sci.gsfc.nasa.gov/measures/documentation/Science_of_the_data.GSSTF2c.pdf>

Shie, C.-L., and K. A. Hilburn (2011), A satellite-based global ocean surface turbulent fluxes dataset and the impact of the associated SSM/I brightness temperature, Proceedings of the 2011 EUMESAT Meteorological Satellite Conference, 8 pp, EMETSAT, Darmstadt, Germany.

Shie, C.-L., K. A. Hilburn, L. S. Chiu, R. Adler, I-I Lin, E. Nelkin, and J. Ardizzone (2011), The Goddard Satellite-Based Surface Turbulent Fluxes Dataset --- Version 2c (GSSTF2c). In: NASA GES DISC, October 2011, Available from <ftp://aurapar1u.ecs.nasa.gov/data/s4pa/GSSTF/> or http://disc.sci.gsfc.nasa.gov/daac-bin/DataHoldingsMEASURES.pl?PROGRAM_List=ChungLinShie

Tomita, H., M. Kubota, M. F. Cronin, S. Iwasaki, M. Konda, and H. Ichikawa (2010), An assessment of surface heat fluxes from J-OFURO2 at the KEO and JKEO sites, *J. Geophys. Res.*, *115*, C03018, doi:10.1029/2009JC005545.

Wentz, F. J. (1997), A well-calibrated ocean algorithm for special sensor microwave / imager, *J. Geophys. Res.*, *102*(C4), 8703–8718, doi:10.1029/96JC01751.

Wentz, F. J., and T. Meissner (2000), AMSR Ocean Algorithm, Version 2, report number 121599A-1, 66 pp, Remote Sensing Systems, Santa Rosa, CA.

Wentz, F. J., L. Ricciardulli, K. Hilburn, and C. Mears (2007), How much more rain will global warming bring?, *Science*, *317*, 233–235, doi:10.1126/science.1140746.

Woodruff, S. D., S. J. Worley, S. J. Lubker, Z. Ji, J. E. Freeman, D. I. Berry, P. Brohan, E. C. Kent, R. W. Reynolds, S. R. Smith, and C. Wilkinson (2011), ICOADS Release 2.5: extensions and enhancements to the surface marine meteorological archive, *Int. J. Climatol.*, *31*, 951–967, doi: 10.1002/joc.2103.

Xing, Y. (2006), Recent changes in oceanic latent heat flux from remote sensing. Ph.D. dissertation, 119 pp, School of Computational Science, George Mason University, Fairfax, Virginia.

Yu, L. (2007), Global Variations in Oceanic Evaporation (1958–2005): The Role of the Changing Wind Speed, *J. Climate*, *20*, 5376–5390, doi: 10.1175/2007JCLI1714.1.

Yu, L., and R. A. Weller (2007), Objectively Analyzed Air–Sea Heat Fluxes for the Global Ice-Free Oceans (1981–2005), *Bull. Amer. Meteor. Soc.*, *88*, 527–539, doi: 10.1175/BAMS-88-4-527.

Zeng, X., M. Zhao, and R. E. Dickinson (1998), Intercomparison of bulk aerodynamic algorithms for the computation of sea surface fluxes using TOGA COARE and TAO data, *J. Climate*, *11*, 2628–2644, doi: 10.1175/1520-0442(1998)011<2628:IOBAAF>2.0.CO;2.